

Dissipative Floquet Topological Systems

Hossein Deghani¹, Takashi Oka², and Aditi Mitra¹

¹ *Department of Physics, New York University, 4 Washington Place, New York, NY 10003, USA*

² *Department of Applied Physics, University of Tokyo, Hongo 7-3-1, Bunkyo, Tokyo 113-8656, Japan*

(Dated: November 15, 2021)

Motivated by recent pump-probe spectroscopies, we study the effect of phonon dissipation and potential cooling on the nonequilibrium distribution function in a Floquet topological state. To this end, we apply a Floquet kinetic equation approach to study two dimensional Dirac fermions irradiated by a circularly polarized laser, a system which is predicted to be in a laser induced quantum Hall state. We find that the initial electron distribution shows an anisotropy with momentum dependent spin textures whose properties are controlled by the switching-on protocol of the laser. The phonons then smoothen this out leading to a non-trivial isotropic nonequilibrium distribution which has no memory of the initial state and initial switch-on protocol, and yet is distinct from a thermal state. An analytical expression for the distribution at the Dirac point is obtained that is relevant for observing quantized transport.

PACS numbers: 73.43.-f, 05.70.Ln, 03.65.Vf, 72.80.Vp

I. INTRODUCTION

Recent years have seen the emergence of topological states of matter which is a new way of characterizing materials by the geometric properties of the underlying band-structure.¹⁻⁵ These include time reversal (TR) breaking integer quantum Hall systems, TR preserving spin quantum Hall systems or two-dimensional (2D) topological insulators (TIs), 3D TIs, and their strongly interacting counterparts.⁶ Another intriguing class of systems are those that can show topological behavior only under out of equilibrium conditions, the main candidate being the Floquet TIs which arise under periodic driving.⁷⁻¹⁵

Consider a time periodic Hamiltonian $H(t) = H(t+T)$ where the periodicity may be due to an external irradiation by a laser. Then the time-evolution over one period can be written as $U(t+T, t) = e^{-iH_F T}$ where H_F is the Floquet Hamiltonian: an effective time-independent Hamiltonian that captures the stroboscopic time-evolution over one period.^{16,17} Floquet TIs have been mainly described by borrowing concepts from equilibrium where the topological properties are extracted by analyzing the spectrum of H_F , with the topological phase showing non-zero Chern numbers and edge-states, though the precise correspondence between the usual equilibrium definition of the Chern number and the number of edge-states does not always work.¹⁸⁻²⁰ Experimentally Floquet TIs have been realized in a photonic system which is effectively in equilibrium because the periodicity in time is replaced by a periodicity in position.²¹ A Floquet TI has also been realized in a periodically modulated honeycomb optical lattice of fermionic atoms,²² where in the limit of high frequency of modulations, the Floquet Hamiltonian maps onto the Haldane model.¹

However Floquet TIs are manifestly out of equilibrium and so raise a unique set of questions that do not arise in systems in equilibrium, one of them being the issue of the electron distribution function, critical for determin-

ing measurable quantities. Obviously the distribution function, at least in ideal closed quantum systems, will depend on how the periodic driving is switched on²³⁻²⁵ where any switching-on protocol breaks time-periodicity. In addition the occupation probability will be very sensitive to any coupling to an external reservoir.²⁶⁻²⁸ Often reservoir engineering can even produce topological properties absent in the closed system,^{29,30} which in turn requires new measures for topological order in open and dissipative systems.³¹⁻³³

The main aim of this paper is to understand the electron distribution function of Floquet topological systems by accounting for the initial switching-on protocol of the periodic drive and accounting for coupling to a reservoir of phonons. We will derive and solve a kinetic equation for the electron distribution function, and show that the combined effect of drive and dissipation can stabilize non-trivial steady-states. We will discuss the signature of these states on spin and angle resolved photoemission (ARPES).

The outline of the paper is as follows, in Section II the model is introduced, in Section III physical quantities are calculated for the closed system and for a quench switching-on protocol of the laser. In Section IV we generalize to the open system where the electrons are coupled to a phonon reservoir. The rate or kinetic equation accounting for inelastic electron-phonon scattering in the presence of a periodic drive is derived, the results for physical quantities at steady-state are obtained and compared with results for the closed system. Finally in section V we present our conclusions. Derivation of general expressions for the Green's functions needed for ARPES is given in Appendix A. Analytic results can be obtained in the vicinity of the Dirac point for both the closed and the open system, and these are derived in Appendices B and C respectively.

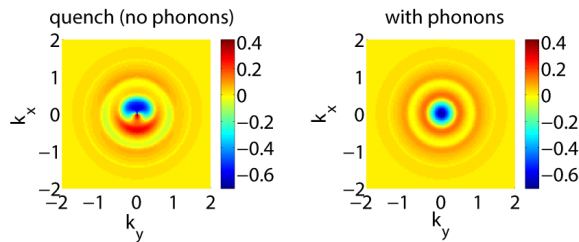


FIG. 1. (color online) Contour plots for the time-averaged spin density $P_z(k_x, k_y)$. Left panel: Without phonons and for a quench. Right panel: At steady-state with phonons. $A_0/\Omega = 0.5$, $\lambda^2 D_{\text{ph}} = 0.1\Omega$, $T = 0.01\Omega$, $\Omega = 1$.

II. MODEL

We study 2D Dirac fermions coupled to an external circularly polarized laser, and also coupled to a bath of phonons. The Hamiltonian is,

$$H = H_{\text{el}} + H_{\text{ph}} + H_c \quad (1)$$

where (setting $\hbar = 1$)

$$H_{\text{el}} = \sum_{\vec{k}=[k_x, k_y], \sigma, \sigma'=\uparrow, \downarrow} c_{\vec{k}\sigma}^\dagger \left[\vec{k} + \vec{A}(t) \right] \cdot \vec{\sigma}_{\sigma\sigma'} c_{\vec{k}\sigma'} \quad (2)$$

$c_{\vec{k}\sigma}^\dagger, c_{\vec{k}\sigma}$ are creation, annihilation operators for the Dirac fermions whose velocity $v = 1$, $\vec{\sigma} = [\sigma_x, \sigma_y]$ are the Pauli matrices, $\vec{A} = \theta(t)A_0 [\cos(\Omega t), -\sin(\Omega t)]$ is the circularly polarized laser which has been suddenly switched on at time $t = 0$, we will refer to this switch-on protocol as a quench. This model plays a central role in the study of Floquet topological states where the circularly polarized laser generates a mass term $m\sigma_z$ in the Floquet Hamiltonian H_F ,^{7,11} with $m = \frac{A_0^2}{\Omega}$ in the high-frequency limit of $A_0/\Omega \ll 1$. This implies a Hall conductivity $\sigma_{xy} = \text{sign}(m)e^2/2h$ provided a zero temperature equilibrium distribution at half-filling is realized. H_F is also the continuum limit of the Haldane model¹ which is an example of a TI (Chern insulator), and was recently realized experimentally using optical lattices.²² Gapless surface states of a 3D TI are also modeled by the Dirac Hamiltonian, and were recently studied by pump-probe spectroscopy,^{34,35} while laser induced Hall effect and chiral edge states are being experimentally studied in graphene.^{36,37}

Dissipation affects the electron distribution and thus the topological signatures. Here we consider dissipation due to coupling to 2D phonons

$$H_{\text{ph}} = \sum_{q, i=x, y} \left[\omega_{qi} b_{qi}^\dagger b_{qi} \right] \quad (3)$$

For now we do not specify whether we have acoustic or optical phonons, and hence the particular form of the

dispersion ω_{qi} . We will specify this when presenting our results. The electron-phonon coupling is

$$H_c = \sum_{\vec{k}, q, \sigma, \sigma'} c_{\vec{k}\sigma}^\dagger \vec{A}_{\text{ph}}(q) \cdot \vec{\sigma}_{\sigma\sigma'} c_{\vec{k}\sigma'} \quad (4)$$

$$\vec{A}_{\text{ph}}(q) = [\lambda_{x,q} (b_{x,q}^\dagger + b_{x,-q}), \lambda_{y,q} (b_{y,q}^\dagger + b_{y,-q})] \quad (5)$$

Above we neglect phonon induced scattering between electrons with different momenta. This simplifies the kinetic equation for the electron distribution function considerably, without changing the physics, and is a microscopic way of accounting for a Caldeira-Leggett³⁸ type dissipation. In Section III, we will first discuss the physics in the absence of the phonons $H_c = 0$, but accounting for the sudden switch-on protocol of the laser, presenting results for the steady-state distribution function and Green's functions, quantities that are measured in ARPES. In Section IV we will address how the results get modified due to coupling to phonons.

III. RESULTS FOR THE QUENCH AND IN THE ABSENCE OF PHONONS

Suppose that at $t \leq 0$, there is no external irradiation, and the electrons are in the ground-state, *i.e.*, all states below the Dirac point are occupied. Thus the wavefunction right before the switching on of the laser is

$$|\Psi_{\text{in}}(t = 0^-)\rangle = \prod_{\vec{k}} |\psi_{\text{in}, \vec{k}}\rangle$$

$$|\psi_{\text{in}, \vec{k}}\rangle = \frac{1}{\sqrt{2}} \begin{pmatrix} -e^{-i\theta_{\vec{k}}} \\ 1 \end{pmatrix} \quad (6)$$

where $\theta_{\vec{k}} = \arctan(k_y/k_x)$. The time-evolution after switching on the laser is

$$|\Psi(t > 0)\rangle = U_{\text{el}}(t, 0) |\Psi_{\text{in}}\rangle \quad (7)$$

where $U_{\text{el}}(t, t')$ is the time-evolution operator,

$$i \frac{dU_{\text{el}}(t, t')}{dt} = H_{\text{el}}(t) U_{\text{el}}(t, t') ; U_{\text{el}}(t, t) = 1 \quad (8)$$

Since we neglect any spatial dependence of the laser field, the system stays translationally invariant. Thus the dynamics is factorizable between different momenta, $U_{\text{el}}(t, t') = \prod_{\vec{k}} U_{\vec{k}}(t, t')$ so that, $|\Psi(t)\rangle = \prod_{\vec{k}} |\psi_{\vec{k}}(t)\rangle = \prod_{\vec{k}} U_{\vec{k}}(t, 0) |\psi_{\text{in}, \vec{k}}\rangle$, where

$$U_{\vec{k}}(t, t') = \sum_{\alpha=\pm} |\psi_{\vec{k}\alpha}(t)\rangle \langle \psi_{\vec{k}\alpha}(t')| \quad (9)$$

$|\psi_{\vec{k}\alpha}(t)\rangle$ being the exact solution of the Schrödinger equation which may be written in terms of the time-periodic Floquet quasi-modes ($|\phi_{\vec{k}\alpha}(t+T)\rangle = |\phi_{\vec{k}\alpha}(t)\rangle$) and quasi-energies ($\epsilon_{\vec{k}\alpha}$) as follows,

$$|\psi_{\vec{k}\alpha}(t)\rangle = e^{-i\epsilon_{\vec{k}\alpha}t} |\phi_{\vec{k}\alpha}(t)\rangle$$

$$[H_{\text{el}} - i\partial_t] |\phi_{\vec{k}\alpha}\rangle = \epsilon_{\vec{k}\alpha} |\phi_{\vec{k}\alpha}\rangle \quad (10)$$

The quasi-energies $\epsilon_{k\alpha}$ represent an infinite ladder of states where $\epsilon_{k\alpha}$ and $\epsilon_{k\alpha} + m\Omega$, for m any integer, represent the same physical state corresponding to the Floquet quasi-modes $|\phi_{k\alpha}(t)\rangle$ and $e^{im\Omega t}|\phi_{k\alpha}(t)\rangle$. Confusion due to this over-counting can be easily avoided by noting that in all physical quantities, including the matrix elements for electron-phonon scattering that enter the kinetic equation, it is always the combination $e^{-i\epsilon_{k\alpha}t}|\phi_{k\alpha}(t)\rangle = |\psi_{k\alpha}\rangle$ that appears, where there are only two distinct states corresponding to $\alpha = \pm$. However while in a typical two-level system, there is only one energy-scale corresponding to the level splitting, in this problem, a hierarchy of energy scales $\epsilon_{k+} - \epsilon_{k-} + m\Omega$ are possible, although one needs to take care that not all matrix elements for inelastic processes at these energy-scales may exist. This will be discussed in more detail below when we present our results.

We can determine the retarded Green's function³⁹

$$\begin{aligned} g_{\sigma\sigma'}^R(k, t, t') &= -i\theta(t-t')\langle\Psi_{\text{in}}|\left\{c_{k\sigma}(t), c_{k\sigma'}^\dagger(t')\right\}|\Psi_{\text{in}}\rangle \\ &= -i\theta(t-t')U_{k,\sigma\sigma'}(t, t') \end{aligned} \quad (11)$$

and the lesser Green's function,

$$\begin{aligned} g_{\sigma\sigma'}^<(k, t, t') &= -i\langle\Psi_{\text{in}}|c_{k\sigma}^\dagger(t)c_{k\sigma'}(t')|\Psi_{\text{in}}\rangle \\ &= -i\sum_{\sigma_1, \sigma_2} \langle\Psi_{\text{in}}|c_{k\sigma_2}^\dagger c_{k\sigma_1}|\Psi_{\text{in}}\rangle U_{k,\sigma_2\sigma}(0, t)U_{k,\sigma_1\sigma'}(t', 0) \end{aligned} \quad (12)$$

While g^R does not depend on the occupation probability (by not depending on the initial state), $g^<$ depends on it. We perform a Fourier transformation of the Green's functions $g(k, t, t')$ with respect to the time-difference $t - t'$ thus moving to the frequency ω space, and all throughout we present results after time-averaging over the mean time $T_m = (t + t')/2$. Thus in what follows, whenever we denote quantities by the arguments k, ω alone, it should be understood that an averaging over mean time T_m has already been performed. General expressions for the Green's functions are presented in Appendix A where the averaging procedure over the mean time is also explained.

We refer to $ig_{\sigma\sigma'}^<(k, \omega)$ as the spin resolved ARPES spectrum, a key quantity in this work that can be directly probed in experiments.³⁴ Note that results for the spectral density $A = \text{Im}[g^R]$ have been discussed elsewhere^{7,39}, however our results for $g^<$ even in the absence of phonons are new. We note that number conservation, absence of momentum mixing, and the fact that we are at half-filling imply the sum rule $\int(d\omega/2\pi)i\sum_{\sigma}g_{\sigma\sigma}^<(k, \omega) = 1$.

The results for the momentum dependent spin-density $P_z(k, T_m) = i\sum_{\sigma}\sigma g_{\sigma\sigma}^<(k, T_m, T_m)$ after averaging over T_m is shown as a contour plot in the left panel of Fig. 1 as well as along the line $k_y = 0$ in Fig. 2. The circularly polarized laser induces a strongly momentum dependent spin density which shows oscillations each time the condition for a photon induced resonance between

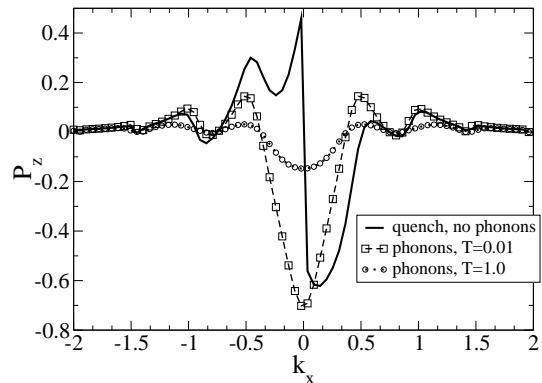


FIG. 2. Spin density $P_z(k_x, k_y = 0)$ for $A_0/\Omega = 0.5$, $\Omega = 1.0$, $\lambda^2 D_{\text{ph}} = 0.1\Omega$ for three different cases: for the quench with no phonons, steady-state with phonons at temperature $T = 0.01\Omega$, and $T = \Omega$.

the Dirac bands $|k| \simeq n\Omega/2$, where n is an integer, is obeyed. Further, the density is also anisotropic in momentum space. The spin averaged ARPES spectrum $ig_{\text{tot}}^<(k, \omega) = i\sum_{\sigma}g_{\sigma\sigma}^<(k, \omega)$ is plotted as an intensity plot in Fig. 3 and its momentum slices in Fig. 4. Note that the delta-functions are given an artificial broadening which is such that the heights of the peaks in Fig. 4 equal the prefactor of the delta function. In other words, $B\pi\delta(\omega - \epsilon_k)$ has been approximated by $\frac{B}{\gamma} \frac{\gamma^2}{\gamma^2 + (\omega - \epsilon_k)^2}$ with the broadening γ arbitrary and chosen so that the plots are visible. Moreover we plot γg (or γG with phonons), so that the height of the peaks in Fig. 4 equals the prefactor of the δ -function B .

The ARPES spectrum clearly shows the appearance of Floquet bands. Without phonons, the system is free, and the electron distribution is given by the overlap $|\langle\phi_{k\alpha=\pm}(0)|\psi_{\text{in},k}\rangle|^2$. This is a highly non-thermal state that retains memory of the initial state $|\psi_{\text{in},k}\rangle$, and is not expected to thermalize. Just like the spin resolved density, the total density in Fig. 3 shows a clear asymmetry under $k_x \rightarrow -k_x$, where this particular anisotropy is determined by the phase of the AC field at $t = 0^+$. Note that in our case, initially the gauge field $\vec{A}(t = 0^+) = [A_0, 0]$ is entirely along the \hat{x} direction.

The anisotropy can be understood analytically at $k=0$ (see Appendix B for details),

$$P_z(k = 0, \theta_k) = -\frac{2A_0\Omega}{\Delta^2} \cos \theta_k; \Delta = \sqrt{4A_0^2 + \Omega^2} \quad (13)$$

where θ_k is the angle along which $k = 0$ is approached. This has the same anisotropy as the left panel in Fig. 1.

For the lesser Green's function at $k=0$ we obtain,

$$\begin{aligned}
 ig_{\sigma\sigma}^<(k=0, \theta_k, \omega) &= 2\pi \sum_{\alpha=\pm} \rho_{k=0, \alpha\alpha}^{\text{quench}} \\
 &\times \left[\left(\frac{\Delta + \alpha\sigma\Omega}{2\Delta} \right) \delta \left(\omega + \sigma \frac{(\alpha\Delta + \Omega)}{2} \right) \right], \\
 \rho_{k=0, \alpha\alpha}^{\text{quench}} &= |\langle \phi_{k=0, \alpha}(0) | \psi_{\text{in}, k=0} \rangle|^2 = \frac{1}{2} \left(1 - \frac{2\alpha A_0}{\Delta} \cos \theta_k \right)
 \end{aligned} \tag{14}$$

above $\sigma = +/ -$ for \uparrow / \downarrow . The analytic expression for $g^<$ shows that for $k=0$, there are exactly four resonances for inelastic scattering, where the two resonances for spin σ occur at $\omega = -\sigma(\Omega \pm \Delta)/2$. Naively one would have expected infinite number of resonances $\epsilon_{k+} - \epsilon_{k-} + m\Omega$ for integer m . The fact that at $k=0$ there are so few is due to vanishing matrix elements alluded to above. As k increases, more and more resonances appear, however they are very rapidly suppressed for large $|m|$.

The above location of the resonances also shows that the circularly polarized field acts as an effective magnetic field along \hat{z} ,¹¹ splitting the energies of the up and down spin electrons. In particular in the high frequency ($A_0 \ll \Omega$) limit, the lowest energy excitation is $\Delta - \Omega \simeq 2A_0^2/\Omega$ and involves flipping a spin from \downarrow to \uparrow . However, this is still not a typical two level system, as for $k=0$, there are two energy scales for energy absorption ($\omega > 0$) (and more for $k \neq 0$), rather than just one energy-scale for energy absorption encountered in a conventional two level system.

The analytic results also show that the weights are far from thermal, where by thermal we imply resonances of the form $\delta(\omega - \epsilon_k)n_F(\omega)$, n_F being the Fermi distribution function at some temperature T . Rather the height of the resonances are proportional to amplitude square of the overlap between the initial wavefunction corresponding to the ground state of the Dirac model, and the wavefunctions $|\psi_{k\alpha}\rangle$. Note that the appearance of only a couple of Floquet bands, and momentum anisotropy is consistent with experimental observations.³⁴

IV. RESULTS IN THE PRESENCE OF PHONONS

The above results for the time-averaged distribution functions after a quench are exact and will not evolve in time. However if we turn on the electron-phonon coupling, inelastic scattering will cause the distribution functions to relax, we now study how this happens, and what is the resulting steady-state. We first briefly outline the derivation of the kinetic or rate equation in the presence of phonons within the Floquet formalism (see⁴⁰ for general discussions). Let $W(t)$ be the density matrix obeying

$$\frac{dW(t)}{dt} = -i[H, W(t)] \tag{15}$$

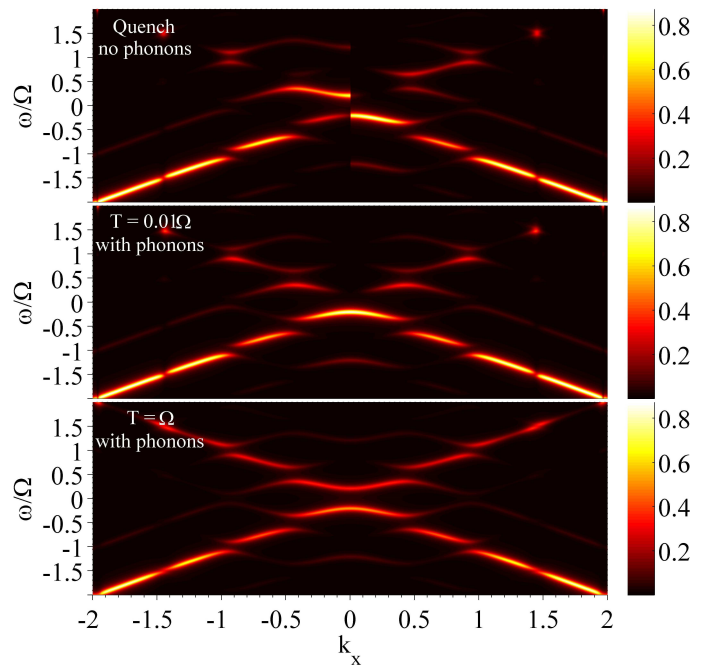


FIG. 3. (color online) Intensity plot of the spin-averaged ARPES spectrum $iG_{\text{tot}}^<(k, \omega)/2$ at $k_y = 10^{-4}$ for the quench with no phonons (upper panels) and at steady-state with phonons at temperature $T = 0.01\Omega, 1\Omega$ (middle and lower panels). $A_0/\Omega = 0.5, \lambda^2 D_{\text{ph}} = 0.1\Omega, \Omega = 1.0$.

It is convenient to be in the interaction representation, $W_I(t) = e^{iH_{\text{ph}}t} U_{\text{el}}^\dagger(t, 0) W(t) U_{\text{el}}(t, 0) e^{-iH_{\text{ph}}t}$. To $\mathcal{O}(H_c^2)$, the density matrix obeys the following equation of motion

$$\begin{aligned}
 \frac{dW_I}{dt} &= -i[H_{c,I}(t), W_I(t_0)] \\
 &- \int_{t_0}^t dt' [H_{c,I}(t), [H_{c,I}(t'), W_I(t')]]
 \end{aligned} \tag{16}$$

where $H_{c,I}$ is in the interaction representation. We assume that at the initial time t_0 , the electrons and phonons are uncoupled so that $W(t_0) = W_0^{\text{el}}(t_0) \otimes W^{\text{ph}}(t_0)$, and that initially the electrons are in the state $|\Psi(t)\rangle$ described in Section III, while the phonons are in thermal equilibrium at temperature T . This is justified because phonon dynamics is much slower than electron dynamics. Thus the quench state of Section III can be achieved within femto-second time-scales,³⁴ while, the phonons do not affect the system until pico-second time-scales.

Thus,

$$W_0^{\text{el}}(t) = |\Psi(t)\rangle \langle \Psi(t)| = \prod_k W_{k,0}^{\text{el}} \tag{17}$$

where

$$W_{k,0}^{\text{el}}(t) = \sum_{\alpha, \beta=\pm} e^{-i(\epsilon_{k\alpha} - \epsilon_{k\beta})t} |\phi_{k\alpha}(t)\rangle \langle \phi_{k\beta}(t)| \rho_{k, \alpha\beta}^{\text{quench}} \tag{18}$$

with

$$\rho_{k, \alpha\beta}^{\text{quench}} = \langle \phi_{k\alpha}(0) | \psi_{\text{in}, k} \rangle \langle \psi_{\text{in}, k} | \phi_{k\beta}(0) \rangle \tag{19}$$

Defining the electron reduced density matrix as the one obtained from tracing over the phonons, $W^{\text{el}} = \text{Tr}_{\text{ph}} W$, and noting that H_c being linear in the phonon operators, the trace vanishes, we need to solve,

$$\frac{dW_I^{\text{el}}}{dt} = -\text{Tr}_{\text{ph}} \int_{t_0}^t dt' [H_{c,I}(t), [H_{c,I}(t'), W_I(t')]] \quad (20)$$

We assume that the phonons are an ideal reservoir and stay in equilibrium. In that case $W_I(t) = W_I^{\text{el}}(t) \otimes e^{-H_{\text{ph}}/T} / \text{Tr} [e^{-H_{\text{ph}}/T}]$ (we set $k_B = 1$).

The most general form of the reduced density matrix for the electrons is

$$W_I^{\text{el}}(t) = \prod_k \sum_{\alpha\beta} \rho_{k,\alpha\beta}(t) |\phi_{k,\alpha}(t)\rangle \langle \phi_{k,\beta}(t)| \quad (21)$$

where in the absence of phonons, $\rho_{k,\alpha\beta} = \rho_{k,\alpha\beta}^{\text{quench}}$ and are time-independent in the interaction representation. The last remaining assumption is to identify the slow and fast variables, which allows one to make the Markov approximation.⁴⁰ We write $\rho_{k,\alpha\beta}(t) = \sum_{m=\text{int}} e^{im\Omega t} \rho_{k,\alpha\beta}^{(m)}(t)$ where in what follows we assume that $\rho_{k,\alpha\beta}^{(m)}(t)$ are slowly varying on time scales of the period of the AC field and the relevant phonon frequencies. In addition we only study the diagonal components of $\rho_{k,\alpha\alpha}^{(m)}$, which after the Markov approximation, obey the rate equation

$$\left[\dot{\rho}_{k,\alpha\alpha}^{(m)}(t) + im\Omega \rho_{k,\alpha\alpha}^{(m)}(t) \right] = - \sum_{m',\beta=\pm} L_{k,\alpha\beta}^{m,m'} \rho_{k,\beta\beta}^{(m-m')}(t) \quad (22)$$

The initial condition we will consider corresponds to a quench switch on protocol for the laser $\rho_{k,\alpha\alpha}^{(m)}(t=0) = \delta_{m=0} \rho_{k,\alpha\alpha}^{\text{quench}}$, with the in-scattering and out-scattering rates $L_{k,\alpha\beta}^{m,m'}$ given in Appendix C.

Since the rate equation is a weak-coupling quasi-classical approximation in the electron-phonon coupling, the position of the resonances in the spectral density are not modified, and thus even with phonons, g^R is unchanged. The phonons strongly modify the steady-state lesser Green's function because the distribution function of the electrons is changed due to inelastic scattering with phonons. In the numerical solutions for the rate equation we assume optical phonons with a uniform phonon density of states D_{ph} , with a broad band-width so that inelastic scattering is always possible. We also assume an isotropic electron-phonon coupling $\lambda_x = \lambda_y = \lambda$. The results can easily be generalized to optical phonons with narrow band-widths, as for frequencies below or above the optical phonon frequencies, the distribution function will remain unchanged, and will be given by that for the quench.

The time-evolution of the density matrix from a quench-type initial state is shown in Fig. 5, where the rate for reaching steady-state is set by the strength of the electron-phonon coupling $\lambda^2 D_{\text{ph}}$. In what follows, we present results for $G^<$ at long times when a steady-state has been reached. The solution of the rate equations

in Fig. 5 shows that the steady-state is characterized by some oscillations with time (controlled by $\lambda^2 D_{\text{ph}}$), and our results are presented after a time-averaging of $\rho_{k,\alpha\alpha}(t) = \rho_{k,\alpha\alpha}^{\text{ss}}$ over several cycles. After this time-averaging, the steady-state lesser Green's function in the presence of phonons is given by,

$$G_{\sigma\sigma'}^<(k, t, t') = -i \sum_{\alpha=\pm} \left[\rho_{k,\alpha\alpha}^{\text{ss}} \langle \phi_{k,\alpha}(0) | c_{k\sigma}^\dagger(t) c_{k\sigma'}(t') | \phi_{k,\alpha}(0) \rangle \right] \quad (23)$$

where $c_{k\sigma}(t) = \sum_{\sigma'} U_{k\sigma\sigma'}(t, 0) c_{k\sigma'}(0)$. Note that due to the laser field, $G^<$ is not time-translationally invariant, and so we average over the mean time $(t + t')/2$ in a manner similar to that done in Section III.

Remarkably, for $k = 0$, $L_{k=0,\alpha\beta}^{m,m'} = \delta_{m,m'} L_{k=0,\alpha\beta}^m$, so that again analytic results are possible. Here we find for the spin-density at $k = 0$,

$$P_z(k=0; H_c \neq 0) = \frac{-2\Omega (\Delta^2 + \Omega^2) / \Delta}{\sum_{\alpha=\pm} (\Delta - \alpha\Omega)^2 \left\{ 1 + 2N(\Delta + \alpha\Omega) \right\}} \quad (24)$$

where $N(x)$ is the Bose distribution function, while

$$iG_{\sigma\sigma'}^<(k=0, \omega; H_c \neq 0) = 2\pi \sum_{\alpha=\pm} \rho_{k=0,\alpha\alpha}^{\text{ss}} \times \left[\left(\frac{\Delta + \alpha\sigma\Omega}{2\Delta} \right) \delta \left(\omega + \sigma \frac{(\alpha\Delta + \Omega)}{2} \right) \right] \quad (25)$$

where⁴¹

$$\rho_{k=0,++}^{\text{ss}} = \frac{\sum_{\beta=\pm} (\Delta - \beta\Omega)^2 N(\Delta + \beta\Omega)}{\sum_{\alpha=\pm} (\Delta - \alpha\Omega)^2 (1 + 2N(\Delta + \alpha\Omega))} \quad (26)$$

with $\sum_{\alpha=\pm} \rho_{k=0,\alpha\alpha}^{\text{ss}} = 1$. Note that the above results at $k = 0$ are isotropic in being independent of the angle θ_k . Thus the coupling to phonons makes the electrons lose memory of the initial state as well as the initial switch-on protocol for the laser. This results in a symmetric distribution of the density in momentum space. This is also clearly seen in the contour plot of Fig. 1. Fig. 2 shows that the spin-density still retains oscillations at momenta k for which the photon frequencies are resonant with the Dirac bands, however the magnitude of the oscillations decay with increasing temperature of the phonon bath, with the spin-density $P_z(k)$ approaching zero as the temperature increases.

The spin averaged ARPES spectrum $iG_{\text{tot}}^<$ in the steady-state with phonons is shown as an intensity plot in the middle and lower panels in Fig. 3 and along some momentum slices in Fig. 4. One finds that as the temperature of the phonon bath decreases, the magnitude of the resonances at positive frequencies decrease and the ones at negative frequencies increase, maintaining the sum rule. While this is also the expected result from a simple thermal Green's function where the weights of the resonances are $\delta(\omega - \epsilon_k) n_F(\epsilon_k)$, yet note that the

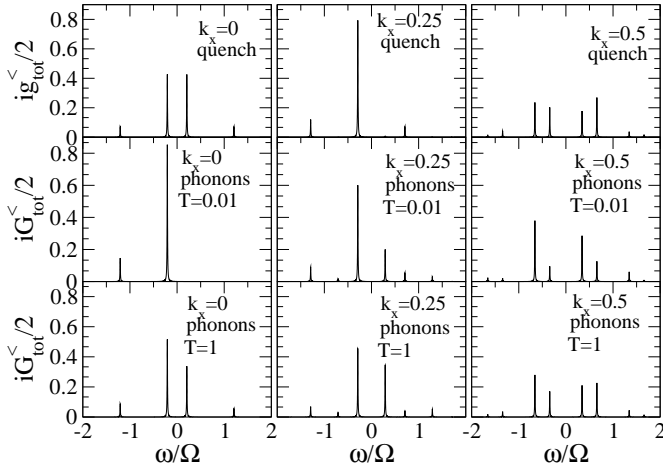


FIG. 4. $iG_{\text{tot}}^<(k, \omega)$ for the quench with no phonons (upper panels) and at steady-state with phonons at temperature $T = 0.01\Omega, 1\Omega$ (middle and lower panels) for $k_y = 10^{-4}$ and $k_x = 0.0, 0.25, 0.5$. $A_0/\Omega = 0.5, \lambda^2 D_{\text{ph}} = 0.1\Omega, \Omega = 1.0$. Normalization such that the peak heights equal the prefactor of the δ -functions.

precise weights in steady-state are not thermal. This can also be clearly seen in the analytic solution for $k = 0$. In particular Eq. (24) implies that in the high frequency limit

$$P_z(k=0, A_0 \ll \Omega) \rightarrow \frac{\tanh[A_0^2/\Omega T]}{[1 + (A_0^4/\Omega^4) \tanh(A_0^2/\Omega T) \coth(\Omega/T)]} \quad (27)$$

In this high-frequency limit, the Floquet Hamiltonian is $H_F \simeq \sigma_x k_x + \sigma_y k_y + \sigma_z A_0^2/\Omega$, so a naive guess would be that the thermalized state should have a magnetization of $\tanh(h_z/2T)$ where $h_z = 2A_0^2/\Omega$. The result for P_z shows deviations from this guess at $\mathcal{O}(A_0^4/\Omega^4)$. Thus, the presence of the AC drive causes the electrons to reach a nonequilibrium steady-state even when the phonon reservoir to which the electrons are coupled are themselves always in thermal equilibrium. Fig. 4 also shows that as k approaches the photon induced resonance condition $|k| \sim n\Omega/2$, the effective temperature is higher, as more frequencies are excited. This result is clearly reflected in Fig. 3 (central panel) where even when the phonon temperature is very low, the avoided crossings are characterized by a high population density.

V. CONCLUSIONS

In summary we have studied the electron distribution in a Floquet topological system under two circumstances, one is for the closed system, where the results are very sensitive to how the AC field has been switched on, showing highly anisotropic distribution functions, the second is for the open system where the electrons are coupled to a reservoir of phonons. While coupling to phonons

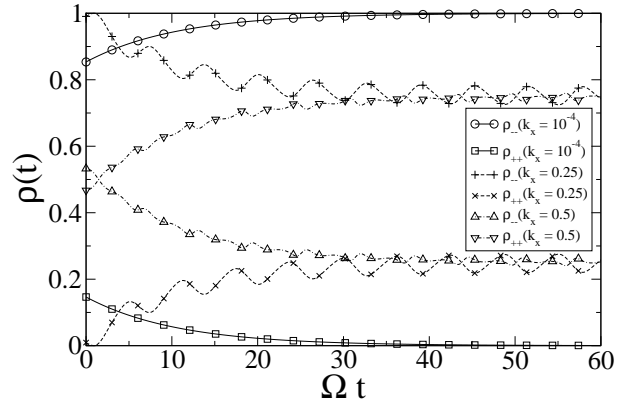


FIG. 5. Time-evolution of $\rho_{k, \alpha \alpha = \pm}$ from an initial state corresponding to a quench for $k_y=0$ and $k_x = 10^{-4}, 0.25, 0.5$. $A_0/\Omega = 0.5, \lambda^2 D_{\text{ph}} = 0.1\Omega, T = 0.01\Omega, \Omega = 1.0$.

causes the system to lose memory of its initial state, yet the presence of the drive gives rise to non-trivial nonequilibrium steady-states observable in ARPES. Since electron dynamics is much faster than phonon dynamics, the results for the quench should be observable on short \sim femto-second time-scales, while the phonons will start relaxing the system on much longer time-scales. The rate equations show that the system will eventually reach a nonequilibrium steady-state with the phonons on time-scales that are inverse of the effective electron-phonon coupling $\mathcal{O}(\lambda^2 D_{\text{ph}})$ which is a highly material dependent parameter, and in realistic materials suggests time-scales of the order of pico-seconds.

An important open question is to understand transport phenomena such as the Hall conductance. Since the Hall response is dominated by the behavior near $k = 0$ where the Berry curvature is peaked, our results imply that the anisotropic distribution of the closed system will cause significant deviation from the quantum limit. On the other hand coupling to low temperature phonons induces cooling of Floquet states. The cooling works efficiently near the Dirac point, which could help the system to approach the quantum limit. However, near resonant points (energy difference $\sim n\Omega$), our results also show that the effective temperature stays high due to photo-carriers. Thus how close the system is to the quantum limit will be a competition between the contribution to the Hall-conductance at the Dirac points, and the role of these excited photo-carriers. A quantitative treatment requires being on the lattice, as in the continuum, the Berry-curvature shows very sharp peaks at the resonances, and becomes mathematically ill-defined. However it is clear that to reach the quantum limit, in addition to having a low temperature bath, it would also be helpful to be in the high frequency regime where Ω is greater than the band-width so as to suppress excited photo-carriers, a regime which is non-existent in the continuum due to the unbounded energy dispersion.

Acknowledgments: This work was supported by US

Department of Energy (DOE-BES) under Award No. DE-SC0010821 (HD and AM), and partially by the Simons Foundation (academic year support for AM).

Appendix A: Green's functions

In this section we highlight how the Green's functions defined in Eqns. (11) and (12) can be obtained. Since the quasi-modes are periodic in time, we may write them as,

$$|\phi_{k\alpha}(t)\rangle = \sum_{m \in \text{int}} e^{im\Omega t} \begin{pmatrix} \alpha_{km\alpha} \\ \beta_{km\alpha} \end{pmatrix} \quad (\text{A1})$$

Thus the time-evolution operator becomes,

$$U_k(t = T_m + \tau/2, t' = T_m - \tau/2) = \sum_{\alpha=\pm, m, m'} e^{-i\epsilon_{k\alpha}\tau + \frac{m+m'}{2}\Omega\tau + i(m-m')\Omega T_m} \times \begin{pmatrix} \alpha_{km\alpha} \\ \beta_{km\alpha} \end{pmatrix} \begin{pmatrix} \alpha_{km'\alpha}^* & \beta_{km'\alpha}^* \end{pmatrix} \quad (\text{A2})$$

Averaging over T_m ,

$$\bar{U}_k(\tau) = \sum_{\alpha=\pm, m} e^{-i\epsilon_{k\alpha}\tau + m\Omega\tau} \begin{pmatrix} \alpha_{km\alpha} \\ \beta_{km\alpha} \end{pmatrix} \begin{pmatrix} \alpha_{km\alpha}^* & \beta_{km\alpha}^* \end{pmatrix} \quad (\text{A3})$$

so that on Fourier transforming with respect to the time difference τ , the retarded Green's function becomes

$$g^R(k, \omega) = \sum_{\alpha, m} \frac{1}{\omega - (\epsilon_{k\alpha} - m\Omega) + i\delta} \times \begin{pmatrix} \alpha_{km\alpha} \\ \beta_{km\alpha} \end{pmatrix} \begin{pmatrix} \alpha_{km\alpha}^* & \beta_{km\alpha}^* \end{pmatrix} \quad (\text{A4})$$

For $k = 0$, analytic expressions for g_R may be obtained and these are presented in Eq. (B24),

For the lesser Green's functions, using Eq. (12), we have,

$$g_{\uparrow\uparrow}^<(k, t, t') = -i \sum_{\alpha, \beta=\pm, m, m', n, n'} e^{-i\epsilon_{k\beta}t' + i\epsilon_{k\alpha}t + in\Omega t' - im\Omega t} \left[\begin{aligned} &\alpha_{kn\beta}\alpha_{kn'\beta}^*\alpha_{km'\alpha}\alpha_{km\alpha}^*\langle c_{k\uparrow}^\dagger c_{k\uparrow} \rangle_0 \\ &+ \alpha_{kn\beta}\beta_{kn'\beta}^*\beta_{km'\alpha}\alpha_{km\alpha}^*\langle c_{k\downarrow}^\dagger c_{k\downarrow} \rangle_0 \\ &+ \alpha_{kn\beta}\alpha_{kn'\beta}^*\beta_{km'\alpha}\alpha_{km\alpha}^*\langle c_{k\downarrow}^\dagger c_{k\uparrow} \rangle_0 \\ &+ \alpha_{kn\beta}\beta_{kn'\beta}^*\alpha_{km'\alpha}\alpha_{km\alpha}^*\langle c_{k\uparrow}^\dagger c_{k\downarrow} \rangle_0 \end{aligned} \right] \quad (\text{A5})$$

and,

$$g_{\downarrow\downarrow}^<(k, t, t') = -i \sum_{\alpha, \beta=\pm, m, m', n, n'} e^{-i\epsilon_{k\beta}t' + i\epsilon_{k\alpha}t + in\Omega t' - im\Omega t} \left[\begin{aligned} &\beta_{kn\beta}\alpha_{kn'\beta}^*\alpha_{km'\alpha}\beta_{km\alpha}^*\langle c_{k\uparrow}^\dagger c_{k\uparrow} \rangle_0 \\ &+ \beta_{kn\beta}\beta_{kn'\beta}^*\beta_{km'\alpha}\beta_{km\alpha}^*\langle c_{k\downarrow}^\dagger c_{k\downarrow} \rangle_0 \\ &+ \beta_{kn\beta}\alpha_{kn'\beta}^*\beta_{km'\alpha}\beta_{km\alpha}^*\langle c_{k\downarrow}^\dagger c_{k\uparrow} \rangle_0 \\ &+ \beta_{kn\beta}\beta_{kn'\beta}^*\alpha_{km'\alpha}\beta_{km\alpha}^*\langle c_{k\uparrow}^\dagger c_{k\downarrow} \rangle_0 \end{aligned} \right] \quad (\text{A6})$$

where $\langle c_{k\sigma}^\dagger c_{k\sigma'} \rangle_0 = \langle \psi_{\text{in}, k} | c_{k\sigma}^\dagger c_{k\sigma'} | \psi_{\text{in}, k} \rangle$ for the closed system with a quench switch-on protocol. For the open system in steady-state, $\langle c_{k\sigma}^\dagger c_{k\sigma'} \rangle_0$ is the average with respect to the steady-state reduced density matrix of the electrons, which is in turn obtained from solving a kinetic equation.

Time-averaging over the mean time $T_m = (t + t')/2$ imposes $\alpha = \beta, m = n$, so that

$$\bar{g}_{\uparrow\uparrow}^<(k, \tau = t' - t) = -i \sum_{\alpha=\pm, n} e^{-i[\epsilon_{k\alpha} - n\Omega]\tau} |\alpha_{kn\alpha}|^2 \rho_{k, \alpha\alpha}$$

$$\bar{g}_{\downarrow\downarrow}^<(k, \tau = t' - t) = -i \sum_{\alpha=\pm, n} e^{-i[\epsilon_{k\alpha} - n\Omega]\tau} |\beta_{kn\alpha}|^2 \rho_{k, \alpha\alpha} \quad (\text{A7})$$

Above $\rho_{k, \alpha\alpha} = |\langle \phi_{k, \alpha}(0) | \psi_{\text{in}, k} \rangle|^2 = \rho_{k, \alpha\alpha}^{\text{quench}}$ for the quench in the closed system, while it is obtained from a kinetic equation for the open system. For the latter, inelastic scattering causes $\rho_{k, \alpha\alpha}$ to evolve in time, and the Markov approximation that we will employ requires that this time-dependence is slow as compared to all other time-scales. For the open system, we will then present results for the Green's functions only at long times, where a steady-state has been reached, where the density matrix is replaced by its steady-state value $\rho_{k, \alpha\alpha} = \rho_{k, \alpha\alpha}^{\text{ss}}$. Sometimes, some slow residual oscillations such as those shown in Fig 5 persist even at long times, in this case such slow oscillations will also be averaged over.

Fourier transforming,

$$ig_{\uparrow\uparrow}^<(k, \omega) = 2\pi \sum_{n\alpha} \delta(\omega - [\epsilon_{k\alpha} - n\Omega]) |\alpha_{kn\alpha}|^2 \rho_{k, \alpha\alpha}$$

$$ig_{\downarrow\downarrow}^<(k, \omega) = 2\pi \sum_{n\alpha} \delta(\omega - [\epsilon_{k\alpha} - n\Omega]) |\beta_{kn\alpha}|^2 \rho_{k, \alpha\alpha} \quad (\text{A8})$$

Analytic expressions for the lesser Green's function for $k = 0$ are given in Eq. (14) for the quench and in Eq. (25) for the steady-state with phonons.

Appendix B: Analytic solution at $k = 0$ for the quench (no phonons)

Let us consider the solution of H_{el} when $k = 0$. In this case, the quasi-modes $|\phi_\alpha\rangle$ (we suppress the $k = 0$ label)

obey the equation,

$$H_{\text{el,F}}(k=0)|\phi_\alpha\rangle = \epsilon_\alpha|\phi_\alpha\rangle \quad (\text{B1})$$

$$H_{\text{el,F}}(k=0) = \vec{A} \cdot \vec{\sigma} - i\partial_t \quad (\text{B2})$$

$$|\phi_\alpha\rangle = \begin{pmatrix} \phi_{\uparrow\alpha} \\ \phi_{\downarrow\alpha} \end{pmatrix} \quad (\text{B3})$$

where $\vec{A} = A_0(\cos\Omega t, -\sin\Omega t)$, so that $\vec{A} \cdot \vec{\sigma} = A_0 \begin{pmatrix} 0 & e^{i\Omega t} \\ e^{-i\Omega t} & 0 \end{pmatrix}$. Thus, the $\phi_{\uparrow,\downarrow\alpha}$ obey the coupled equation

$$-i\partial_t\phi_{\uparrow\alpha} + A_0e^{i\Omega t}\phi_{\downarrow\alpha} = \epsilon_\alpha\phi_{\uparrow\alpha} \quad (\text{B4})$$

$$-i\partial_t\phi_{\downarrow\alpha} + A_0e^{-i\Omega t}\phi_{\uparrow\alpha} = \epsilon_\alpha\phi_{\downarrow\alpha} \quad (\text{B5})$$

Substituting for

$$\phi_{\downarrow\alpha} = \frac{e^{-i\Omega t}}{A_0} [\epsilon_\alpha\phi_{\uparrow\alpha} + i\partial_t\phi_{\uparrow\alpha}] \quad (\text{B6})$$

into the second equation above gives,

$$\partial_t^2\phi_{\uparrow\alpha} - i[2\epsilon_\alpha + \Omega]\partial_t\phi_{\uparrow\alpha} + (A_0^2 - \Omega\epsilon_\alpha - \epsilon_\alpha^2)\phi_{\uparrow\alpha} = 0 \quad (\text{B7})$$

Writing $\phi_{\uparrow\pm} = d_{\uparrow\pm}e^{i\lambda_{\pm}t}$, one obtains $\lambda_{\mp} = \frac{\Omega}{2} + \epsilon_{\mp} \pm \frac{\Delta}{2}$ where

$$\Delta = \sqrt{4A_0^2 + \Omega^2} \quad (\text{B8})$$

Since $\phi_{\uparrow,\downarrow\alpha}(t+T) = \phi_{\uparrow,\downarrow\alpha}(t)$, $\lambda = m\Omega$, where m is an integer. Thus Eq. (B6) gives,

$$\phi_{\downarrow\alpha} = d_{\downarrow\alpha}e^{i(m-1)\Omega t}; \phi_{\uparrow\alpha} = d_{\uparrow\alpha}e^{im\Omega t} \quad (\text{B9})$$

with

$$\epsilon_{\pm} = \left(m - \frac{1}{2}\right)\Omega \pm \frac{\Delta}{2} \quad (\text{B10})$$

$$\frac{d_{\downarrow\pm}}{d_{\uparrow\pm}} = \frac{-\Omega \pm \Delta}{2A_0} \quad (\text{B11})$$

Thus,

$$d_{\uparrow\pm} = \frac{\sqrt{2}A_0}{\sqrt{\Delta(\Delta \mp \Omega)}}; d_{\downarrow\pm} = \pm \frac{1}{\sqrt{2}}\sqrt{1 \mp \frac{\Omega}{\Delta}} \quad (\text{B12})$$

$$|\phi_{\pm}(t)\rangle = e^{im\Omega t} \begin{pmatrix} d_{\uparrow\pm} \\ e^{-i\Omega t}d_{\downarrow\pm} \end{pmatrix} \quad (\text{B13})$$

Note that while there are infinite possible ways to choose the quasi-modes and the corresponding quasi-energies, where the quasi-energies are related by shifts by integer multiples of the frequency Ω , this degeneracy is absent in the wavefunctions corresponding to the exact solutions of the Schrödinger equation, $|\Psi_\alpha(t)\rangle = e^{-i\epsilon_\alpha t}|\phi_\alpha(t)\rangle$. In particular the wavefunctions are

$$|\Psi_+(t)\rangle = e^{i\Omega t/2 - i\Delta t/2} \begin{pmatrix} \frac{\sqrt{2}A_0}{\sqrt{\Delta(\Delta - \Omega)}} \\ e^{-i\Omega t} \frac{1}{\sqrt{2}} \sqrt{1 - \frac{\Omega}{\Delta}} \end{pmatrix} \quad (\text{B14})$$

$$|\Psi_-(t)\rangle = e^{i\Omega t/2 + i\Delta t/2} \begin{pmatrix} \frac{\sqrt{2}A_0}{\sqrt{\Delta(\Delta + \Omega)}} \\ -e^{-i\Omega t} \frac{1}{\sqrt{2}} \sqrt{1 + \frac{\Omega}{\Delta}} \end{pmatrix} \quad (\text{B15})$$

One may also construct the time-evolution operator,

$$\begin{aligned} U_{k=0}(t, t') &= \sum_{\alpha=\pm} e^{-i\epsilon_\alpha(t-t')} |\phi_\alpha(t)\rangle \langle \phi_\alpha(t')| \quad (\text{B16}) \\ &= \sum_{\alpha=\pm} e^{-i\left(\frac{-\Omega+\alpha\Delta}{2}\right)(t-t')} \begin{pmatrix} d_{\uparrow\alpha} \\ e^{-i\Omega t}d_{\downarrow\alpha} \end{pmatrix} (d_{\uparrow\alpha} e^{i\Omega t'} d_{\downarrow\alpha}) \end{aligned} \quad (\text{B17})$$

If the state just before switching on the AC field is the ground state of the Dirac fermions,

$$|\psi_{\text{in}}\rangle = \frac{1}{\sqrt{2}} \begin{pmatrix} -e^{-i\theta_k} \\ 1 \end{pmatrix} \quad (\text{B18})$$

then the wavefunction after the sudden switch-on of the AC field is given by

$$\begin{aligned} |\Psi(t)\rangle &= U_{k=0}(t, 0)|\psi_{\text{in}}\rangle \\ &= \sum_{\alpha=\pm} C_{-\alpha} \frac{\sqrt{\Delta(\Delta - \alpha\Omega)}}{\sqrt{2}A_0} |\Psi_\alpha(t)\rangle \end{aligned} \quad (\text{B19})$$

where

$$C_+ = -\frac{[\omega_- \psi_\uparrow(0) + A_0 \psi_\downarrow(0)]}{(\omega_+ - \omega_-)} \quad (\text{B20})$$

$$C_- = \frac{[\omega_+ \psi_\uparrow(0) + A_0 \psi_\downarrow(0)]}{(\omega_+ - \omega_-)} \quad (\text{B21})$$

with

$$\omega_{\pm} = \frac{\Omega \pm \Delta}{2} \quad (\text{B22})$$

$$\psi_\uparrow(0) = -e^{-i\theta_k}/\sqrt{2}; \psi_\downarrow(0) = 1/\sqrt{2} \quad (\text{B23})$$

Once the wavefunction $|\Psi(t)\rangle$ and the time evolution operator $U(t, t')$ are known, one may compute all the single-time and two-time averages discussed in the main text.

Using the above, and Eq. (A4), the expression for the retarded Green's function is,

$$\begin{aligned} g^R(k=0, \omega) &= \sum_{\alpha=\pm} \frac{1}{\omega - \left(-\frac{\Omega}{2} + \alpha\frac{\Delta}{2}\right) + i\delta} \begin{pmatrix} d_{\uparrow\alpha}^2 & 0 \\ 0 & 0 \end{pmatrix} \\ &+ \sum_{\alpha=\pm} \frac{1}{\omega - \left(\frac{\Omega}{2} + \alpha\frac{\Delta}{2}\right) + i\delta} \begin{pmatrix} 0 & 0 \\ 0 & d_{\downarrow\alpha}^2 \end{pmatrix} \end{aligned} \quad (\text{B24})$$

Using Eq. (A8), the lesser Green's function is given in Eq. (14).

Appendix C: Rate equations for general k and exact solution at $k=0$

The rate equations after the Markov approximation are found to be (below $N_q = N(\omega_q)$ is the Bose distribution function)

$$\begin{aligned}
\left[\dot{\rho}_{k,\alpha\alpha}^{(m)}(t) + im\Omega\rho_{k,\alpha\alpha}^{(m)} \right] = & - \sum_{q,i=x,y,\beta=\pm,n_1,n_2} \left[\pi\lambda_{iq}^2 \left(\epsilon^{i\bar{i}} \left\{ C_{1k\alpha\beta}^{n_1} C_{1k\beta\alpha}^{n_2} + C_{2k\alpha\beta}^{n_1} C_{2k\beta\alpha}^{n_2} \right\} + C_{1k\alpha\beta}^{n_1} C_{2k\beta\alpha}^{n_2} + C_{2k\alpha\beta}^{n_1} C_{1k\beta\alpha}^{n_2} \right) \right] \\
& \times \left[\left\{ (1+N_q)\delta(\epsilon_{k\beta} - \epsilon_{k\alpha} + (m-n_1)\Omega + \omega_{qi}) + N_q\delta(\epsilon_{k\beta} - \epsilon_{k\alpha} + (m-n_1)\Omega - \omega_{qi}) \right\} \rho_{k,\alpha\alpha}^{(m-n_1-n_2)}(t) \right. \\
& - \left\{ (1+N_q)\delta(\epsilon_{k\beta} - \epsilon_{k\alpha} + (m-n_1)\Omega - \omega_{qi}) + N_q\delta(\epsilon_{k\beta} - \epsilon_{k\alpha} + (m-n_1)\Omega + \omega_{qi}) \right\} \rho_{k,\beta\beta}^{(m-n_1-n_2)}(t) \\
& + \left\{ (1+N_q)\delta(\epsilon_{k\beta} - \epsilon_{k\alpha} - (m-n_2)\Omega + \omega_{qi}) + N_q\delta(\epsilon_{k\beta} - \epsilon_{k\alpha} - (m-n_2)\Omega - \omega_{qi}) \right\} \rho_{k,\alpha\alpha}^{(m-n_1-n_2)}(t) \\
& \left. - \left\{ (1+N_q)\delta(\epsilon_{k\beta} - \epsilon_{k\alpha} - (m-n_2)\Omega - \omega_{qi}) + N_q\delta(\epsilon_{k\beta} - \epsilon_{k\alpha} - (m-n_2)\Omega + \omega_{qi}) \right\} \rho_{k,\beta\beta}^{(m-n_1-n_2)}(t) \right] \quad (C1)
\end{aligned}$$

where $\epsilon^{x\bar{x}} = 1, \epsilon^{y\bar{y}} = -1$, and

$$\langle \phi_{k\alpha}(t) | c_{k\uparrow}^\dagger c_{k\downarrow} | \phi_{k\beta}(t) \rangle = \sum_n e^{in\Omega t} C_{1k\alpha\beta}^n \quad (C2)$$

$$\langle \phi_{k\alpha}(t) | c_{k\downarrow}^\dagger c_{k\uparrow} | \phi_{k\beta}(t) \rangle = \sum_n e^{in\Omega t} C_{2k\alpha\beta}^n \quad (C3)$$

1. Analytic results for the rate equation at $k=0$

At $k=0$, the exact expressions for the quasi-modes can be used to show that

$$\langle \phi_\alpha(t) | c_{k=0,\uparrow}^\dagger c_{k=0,\downarrow} | \phi_\beta(t) \rangle = d_{\uparrow\alpha} d_{\downarrow\beta} e^{-i\Omega t} \quad (C4)$$

$$\langle \phi_\alpha(t) | c_{k=0,\downarrow}^\dagger c_{k=0,\uparrow} | \phi_\beta(t) \rangle = d_{\downarrow\alpha} d_{\uparrow\beta} e^{i\Omega t} \quad (C5)$$

Thus, the matrix elements entering the rate equation become,

$$\begin{aligned}
C_{1++}^{(n)} &= \frac{A_0}{\Delta} \delta_{n=-1}; C_{1--}^{(n)} = -\frac{A_0}{\Delta} \delta_{n=-1} \\
C_{1+-}^{(n)} &= -\frac{1}{2} \left(1 + \frac{\Omega}{\Delta} \right) \delta_{n=-1}; C_{1-+}^{(n)} = \frac{1}{2} \left(1 - \frac{\Omega}{\Delta} \right) \delta_{n=-1} \\
C_{2++}^{(n)} &= \frac{A_0}{\Delta} \delta_{n=1}; C_{2--}^{(n)} = -\frac{A_0}{\Delta} \delta_{n=1} \\
C_{2+-}^{(n)} &= \frac{1}{2} \left(1 - \frac{\Omega}{\Delta} \right) \delta_{n=1}; C_{2-+}^{(n)} = -\frac{1}{2} \left(1 + \frac{\Omega}{\Delta} \right) \delta_{n=1}
\end{aligned}$$

Let us assume $\lambda_{xq} = \lambda_{yq}$. In this case for $k=0, n_1+n_2=0$ in the rate equations. So for $k=0$, the rate equations simplify to

$$\begin{aligned}
& \partial_t \begin{pmatrix} \rho_{k=0,++}^{(m)} \\ \rho_{k=0,--}^{(m)} \end{pmatrix} + im\Omega \begin{pmatrix} \rho_{k=0,++}^{(m)} \\ \rho_{k=0,--}^{(m)} \end{pmatrix} \\
& = \begin{pmatrix} L_{k=0,++}^{(m)} & L_{k=0,+ -}^{(m)} \\ L_{k=0,- +}^{(m)} & L_{k=0,--}^{(m)} \end{pmatrix} \begin{pmatrix} \rho_{k=0,++}^{(m)} \\ \rho_{k=0,--}^{(m)} \end{pmatrix} \quad (C6)
\end{aligned}$$

where $L_{k=0,++}^{(m)} = -L_{k=0,-+}^{(m)}; L_{k=0,+ -}^{(m)} = -L_{k=0,--}^{(m)}$. We now make the assumption of a uniform phonon density

of states D_{ph} so that the rates are,

$$\begin{aligned}
L_{k=0,++}^{(m)} &= -\pi\lambda^2 D_{\text{ph}} \frac{1}{2} \left(1 + \frac{\Omega}{\Delta} \right)^2 \left[\right. \\
& \left. \{1 + N(\Delta - \Omega - m\Omega)\} \theta(\Delta - \Omega - m\Omega) \right. \\
& \left. + \{1 + N(\Delta - \Omega + m\Omega)\} \theta(\Delta - \Omega + m\Omega) \right. \\
& \left. + N(-\Delta + \Omega - m\Omega) \theta(-\Delta + \Omega - m\Omega) \right. \\
& \left. + N(-\Delta + \Omega + m\Omega) \theta(-\Delta + \Omega + m\Omega) \right] \\
& -\pi\lambda^2 D_{\text{ph}} \frac{1}{2} \left(1 - \frac{\Omega}{\Delta} \right)^2 \left[\right. \\
& \left. \{1 + N(\Delta + \Omega - m\Omega)\} \theta(\Delta + \Omega - m\Omega) \right. \\
& \left. + \{1 + N(\Delta + \Omega + m\Omega)\} \theta(\Delta + \Omega + m\Omega) \right. \\
& \left. + N(-\Delta - \Omega - m\Omega) \theta(-\Delta - \Omega - m\Omega) \right. \\
& \left. + N(-\Delta - \Omega + m\Omega) \theta(-\Delta - \Omega + m\Omega) \right] \quad (C7)
\end{aligned}$$

and,

$$\begin{aligned}
L_{k=0,--}^{(m)} &= -\pi\lambda^2 D_{\text{ph}} \frac{1}{2} \left(1 - \frac{\Omega}{\Delta} \right)^2 \left[\right. \\
& \left. \{1 + N(-\Delta - \Omega - m\Omega)\} \theta(-\Delta - \Omega - m\Omega) \right. \\
& \left. + \{1 + N(-\Delta - \Omega + m\Omega)\} \theta(-\Delta - \Omega + m\Omega) \right. \\
& \left. + N(\Delta + \Omega - m\Omega) \theta(\Delta + \Omega - m\Omega) \right. \\
& \left. + N(\Delta + \Omega + m\Omega) \theta(\Delta + \Omega + m\Omega) \right] \\
& -\pi\lambda^2 D_{\text{ph}} \frac{1}{2} \left(1 + \frac{\Omega}{\Delta} \right)^2 \left[\right. \\
& \left. \{1 + N(-\Delta + \Omega - m\Omega)\} \theta(-\Delta + \Omega - m\Omega) \right. \\
& \left. + \{1 + N(-\Delta + \Omega + m\Omega)\} \theta(-\Delta + \Omega + m\Omega) \right. \\
& \left. + N(\Delta - \Omega - m\Omega) \theta(\Delta - \Omega - m\Omega) \right. \\
& \left. + N(\Delta - \Omega + m\Omega) \theta(\Delta - \Omega + m\Omega) \right] \quad (C8)
\end{aligned}$$

Above θ is the Heaviside step function.

-
- ¹ F. D. M. Haldane, *Phys. Rev. Lett.* **61**, 2015 (1988).
- ² M. Z. Hasan and C. L. Kane, *Rev. Mod. Phys.* **82**, 3045 (2010).
- ³ X.-L. Qi and S.-C. Zhang, *Rev. Mod. Phys.* **83**, 1057 (2011).
- ⁴ C. L. Kane and E. J. Mele, *Phys. Rev. Lett.* **95**, 146802 (2005).
- ⁵ B. A. Bernevig, T. L. Hughes, and S.-C. Zhang, *Science* **314**, 1757 (2006).
- ⁶ T. Senthil, arXiv:1405.4015 (unpublished).
- ⁷ T. Oka and H. Aoki, *Phys. Rev. B* **79**, 081406 (2009).
- ⁸ J. Inoue and A. Tanaka, *Phys. Rev. Lett.* **105**, 017401 (2010).
- ⁹ T. Kitagawa, E. Berg, M. Rudner, and E. Demler, *Phys. Rev. B* **82**, 235114 (2010).
- ¹⁰ N. H. Lindner, G. Refael, and V. Galitski, *Nature Physics* **7**, 490 (2011).
- ¹¹ T. Kitagawa, T. Oka, A. Brataas, L. Fu, and E. Demler, *Phys. Rev. B* **84**, 235108 (2011).
- ¹² N. H. Lindner, D. L. Bergman, G. Refael, and V. Galitski, *Phys. Rev. B* **87**, 235131 (2013).
- ¹³ A. Gómez-León and G. Platero, *Phys. Rev. Lett.* **110**, 200403 (2013).
- ¹⁴ Y. T. Katan and D. Podolsky, *Phys. Rev. Lett.* **110**, 016802 (2013).
- ¹⁵ P. M. Perez-Piskunow, G. Usaj, C. A. Balseiro, and L. E. F. F. Torres, *Phys. Rev. B* **89**, 121401 (2014).
- ¹⁶ J. H. Shirley, *Phys. Rev.* **138**, B979 (1965).
- ¹⁷ H. Sambe, *Phys. Rev. A* **7**, 2203 (1973).
- ¹⁸ M. S. Rudner, N. H. Lindner, E. Berg, and M. Levin, *Phys. Rev. X* **3**, 031005 (2013).
- ¹⁹ M. Lababidi, I. I. Satija, and E. Zhao, *Phys. Rev. Lett.* **112**, 026805 (2014).
- ²⁰ A. Kundu, H. Fertig, and B. Seradjeh, arXiv:1406.1490 (unpublished).
- ²¹ M. Rechstman, J. Zeuner, Y. Plotnik, Y. Lumer, D. Podolsky, F. Dreisow, S. Nolte, M. Segev, and A. Szameit, *Nature (London)* **496**, 196 (2013).
- ²² G. Jotzu, M. Messer, R. Desbuquois, M. Lebrat, T. Uehlinger, D. Greif, and T. Esslinger, arXiv:1406.7874 (unpublished).
- ²³ A. Lazarides, A. Das, and R. Moessner, *Phys. Rev. Lett.* **112**, 150401 (2014).
- ²⁴ M. A. Sentef, M. Claassen, A. F. Kemper, B. Moritz, T. Oka, J. K. Freericks, and T. P. Devereaux, arXiv:1401.5103 (unpublished).
- ²⁵ N. Goldman and J. Dalibard, *Phys. Rev. X* **4**, 031027 (2014).
- ²⁶ Z. Gu, H. A. Fertig, D. P. Arovas, and A. Auerbach, *Phys. Rev. Lett.* **107**, 216601 (2011).
- ²⁷ A. Kundu and B. Seradjeh, *Phys. Rev. Lett.* **111**, 136402 (2013).
- ²⁸ L. E. F. F. Torres, P. M. Perez-Piskunow, C. A. Balseiro, and G. Usaj, arXiv:1409.2482 (unpublished).
- ²⁹ S. Diehl, E. Rico, M. A. Baranov, and P. Zoller, *Nature Physics* **7**, 971 (2011).
- ³⁰ J. C. Budich, P. Zoller, and S. Diehl, arXiv:1409.6341 (unpublished).
- ³¹ A. Uhlmann, *Rep. Math. Phys.* **24**, 229 (1986).
- ³² A. Rivas, O. Viyuela, and M. A. Martin-Delgado, *Phys. Rev. B* **88**, 155141 (2013).
- ³³ O. Viyuela, A. Rivas, and M. A. Martin-Delgado, *Phys. Rev. Lett.* **112**, 130401 (2014).
- ³⁴ Y. H. Wang, H. Steinberg, P. Jarillo-Herrero, and N. Gedik, *Science* **342**, 453 (2013).
- ³⁵ Y. Onishi, Z. Ren, M. Novak, K. Segawa, Y. Ando, and K. Tanaka, arXiv:1403.2492 (unpublished).
- ³⁶ J. Karch, P. Olbrich, M. Schmalzbauer, C. Zoth, C. Brinsteiner, M. Fehrenbacher, U. Wurstbauer, M. M. Glazov, S. A. Tarasenko, E. L. Ivchenko, D. Weiss, J. Eroms, R. Yakimova, S. Lara-Avila, S. Kubatkin, and S. D. Ganichev, *Phys. Rev. Lett.* **105**, 227402 (2010).
- ³⁷ J. Karch, C. Drexler, P. Olbrich, M. Fehrenbacher, M. Hirmer, M. M. Glazov, S. A. Tarasenko, E. L. Ivchenko, B. Birkner, J. Eroms, D. Weiss, R. Yakimova, S. Lara-Avila, S. Kubatkin, M. Ostler, T. Seyller, and S. D. Ganichev, *Phys. Rev. Lett.* **107**, 276601 (2011).
- ³⁸ A. O. Caldeira and A. J. Leggett, *Phys. Rev. Lett.* **46**, 211 (1981).
- ³⁹ B. M. Fregoso, Y. H. Wang, N. Gedik, and V. Galitski, *Phys. Rev. B* **88**, 155129 (2013).
- ⁴⁰ S. Kohler, J. Lehmann, and P. Hänggi, *Phys. Rep.* **406**, 379 (2005).
- ⁴¹ M. Langemeyer and M. Holthaus, *Phys. Rev. E* **89**, 012101 (2014).